HHS Public Access

Author manuscript

J Am Chem Soc. Author manuscript; available in PMC 2024 April 02.

Published in final edited form as:

J Am Chem Soc. 2023 June 14; 145(23): 12935–12947. doi:10.1021/jacs.3c04393.

Normal and Aberrant Methyltransferase Activities Give Insights into the Final Steps of Dynemicin A Biosynthesis

Paramita Pal,

Department of Chemistry, The Johns Hopkins University, Baltimore, Maryland 21218, United States; Present Address: Takeda Pharmaceuticals, 9625 Towne Centre Drive, San Diego, California 92121, United States

Serena M. L. Wessely,

Department of Chemistry, The Johns Hopkins University, Baltimore, Maryland 21218, United States

Craig A. Townsend

Department of Chemistry, The Johns Hopkins University, Baltimore, Maryland 21218, United States

Abstract

The naturally occurring enediynes are notable for their complex structures, potent DNA cleaving ability, and emerging usefulness in cancer chemotherapy. They can be classified into three distinct structural families, but all are thought to originate from a common linear C_{15}-heptaene. Dynemicin A (DYN) is the paradigm member of anthraquinone-fused enediynes, one of the three main classes and exceptional among them for derivation of both its enediyne and anthraquinone portions from this same early biosynthetic building block. Evidence is growing about how two structurally dissimilar, but biosynthetically related, intermediates combine in two heterodimerization reactions to create a nitrogen-containing C_{30}-coupled product. We report here deletions of two genes that encode biosynthetic proteins that are annotated as *S*-adenosylmethionine (SAM)-dependent methyltransferases. While one, DynO6, is indeed the required *O*-methyltransferase implicated long ago in the first studies of DYN biosynthesis, the other, DynA5, functions in an unanticipated manner in the post-heterodimerization events that complete the biosynthesis of DYN. Despite its removal from the genome of *Micromonospora chersina*, the **Δ***dynA5* strain retains the ability to synthesize DYN, albeit in reduced titers, accompanied by two unusual co-metabolites. We link the appearance of these unexpected structures to a substantial and contradictory body of other recent

Corresponding Author: **Craig A. Townsend** – *Department of Chemistry, The Johns Hopkins University, Baltimore, Maryland 21218, United States*; ctownsend@jhu.edu.

Supporting Information

The Supporting Information is available free of charge at https://pubs.acs.org/doi/10.1021/jacs.3c04393.

Large-scale growth and supplementation of *M. chersina* fermentations and mutant strains with ^{13}C-labeled precursors; isolation, derivatization, and purification of dynemicin A and metabolites accumulated by the Δ*dynO5* and Δ*dynA5* deletion mutants; UV–visible, mass spectrometric, and NMR characterizations of these compounds; list of DNA primers used; gene map comparisons among the known AFE, sungeidine, and calicheamicin BGC's; and the predicted AlphaFold structure of DynO6 and crystal structure of TnmH (PDF)

Complete contact information is available at: https://pubs.acs.org/10.1021/jacs.3c04393

The authors declare no competing financial interest.

experimental data to advance a biogenetic rationale for the downstream steps that lead to the final formation of DYN. A sequence of product-forming transformations that is in line with new and existing experimental results is proposed and supported by a model reaction that also encompasses the formation of the crucial epoxide essential for the activation of DYN for DNA cleavage.

Graphical Abstract

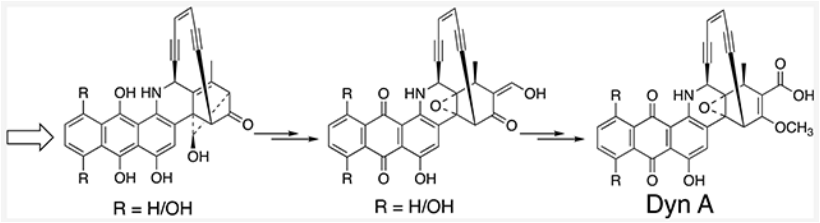

INTRODUCTION

Their fascinating architecture and high cytotoxicity have made enediyne natural products a long-standing target for biosynthetic study and chemotherapeutic drug development. The first reported anthraquinone-containing member of this group, dynemicin A (DYN, **1**),[1] is strikingly dissimilar to the other 10-membered family represented by calicheamicin (CLM, **5**). In recent years, the discovery of new anthraquinone-fused enediynes (AFEs, Figure 1a), uncialamycin (UCL, **2**), tiancimycin (TNM, **3**), and yangpumicin (YPM, **4**), and determination of their biosynthetic gene clusters (BGCs, Figure S1) have drawn increased attention to this class and helped discern both unique and common features among the encoded proteins that create them.[2–5]

The BGC for DYN (**1**) comprises 47 open reading frames spanning over 54 kb. There are high extents of overlap between the DYN and the other four AFE BGC clusters (Figure S1 and Table S6). Principally, the “minimal enediyne cassette” that is well conserved across the BGCs of all known enediynes harbors a highly reducing iterative polyketide synthase, *dynE8*, and a proximal thioesterase (TE), *dynE7*.[6] DYN was recognized early on to be assembled from two polyketide chains on the basis of doubly ^{13}C-labeled acetate incorporation experiments (see Figure 1).[7] The connection between the upper and lower “halves” of 1 takes place through an aryl C–N bond[8–10] and the C8–C9 bond between two C1-labeled acetate carbons, that is, between two intrinsically electrophilic carbons. Equally unexpected, C30 and C5 both derive from C2 of acetate, in contrast to the alternating pattern of acetate C1 and C2 labels emblematic of polyketide biosynthesis. The F-ring methoxy (C31) was demonstrated to derive from the *S*-methyl of methionine, as anticipated.[7]

DynE8 is unusual among the HR-PKSs that lie at the heart of enediyne biosyntheses. It gives rise to both the anthraquinone and enediyne halves of DYN.[11] The HR-PKSs that are central to all studied enediyne biosynthetic pathways have a distinctive domain architecture and common distinguishing features.[12,13] Prominent among them is that a TE domain is typically C-terminal in PKSs and fatty acid synthases but is separately encoded in enediyne genomes and acts in trans to release the β-hydroxyhexaene **6** from the acyl carrier protein (ACP) in a decarboxylative dehydration reaction to the *n*-heptaene **7** (Figure 1b). An early

hypothesis suggested that the in trans competition of the TE with other biosynthetic proteins might account for both the synthesis of heptaene **7** by all examined enediyne producers and the partition of the ACP-bound *β*-hydroxyhexaene, whose ends are functionally differentiated, into the three principal enediyne structural types.[11] In an important recent advance, the linear heptaene was established as the first post-PKS intermediate to ultimately give rise to both halves of DYN (**1**) and quite likely other members of the enediyne natural product family.[14] Notwithstanding intense effort for more than a decade, nothing is known about subsequent enediyne formation in any of these systems beyond **7**.[15] On the other hand, iodoanthracene **8** (Figure 1b), bearing a fused *γ*-thiolactone, is the precursor of the anthraquinone "half" of DYN[16] in steps that ultimately result in all the oxygens in rings A–D being introduced from molecular oxygen,[11] but otherwise the biosynthesis, like its enediyne partner **9**, is wholly unknown.[9]

Bioinformatic analysis of the DYN BGC revealed not one apparent *S*-adenosyl-L-methionine (SAM)-dependent methyltransferase but two, DynO6 and DynA5. DynO6 shows homology to tiancimycin TnmH[12] and calicheamicin CalO6,[17] whose different substrate preferences are well described, as well as yangpumicin YpmJ2, suggesting that DynO6 could prove to be responsible for the introduction of the F-ring methoxy in DYN biosynthesis. All four proteins share high sequence similarity to Class I methyltransferases characterized by a *C*-terminal Rossman fold for SAM binding and a nine-residue consensus sequence with the glycine-rich GxGxG signature present in all SAM-dependent methyltransferases.[18] TnmH, CalO6, and YpmJ2 also share with DynO6 a catalytic His–Asp diad that activates the methyl acceptor to allow for nucleophilic attack on the SAM methyl group (Figure S5). MmcR, another Class I *O*-methyltransferase that shares homology with DynO6, uses Glu313 to help in substrate activation.[19,20] DynO6 shares all three conserved active site residues (His255-Asp256, Glu312), hinting at an analogous mechanism of methylation (Figure S2, green highlighted residues). Other mechanisms of methylation[21] appear unlikely, as an AlphaFold model of DynO6 is highly similar to the X-ray structure of TnmH and reveals a large solvent-accessible cavity that would be suboptimal for a desolvation mechanism, and experiments with the closest homolog TnmH have shown no statistically significant metal ion dependence (Figure S4).[21–23]

By comparison, DynA5 shows low extents of identity to DynO6 in a pairwise alignment with only a partial GxGxG motif indicative of impaired SAM binding, and residues thought to be catalytic (e.g., His255, Asp256, and Glu312 in DynO6) are missing or altered (Figure S3 highlighted in green). Bearing in mind other examples in natural product biosynthesis, bioinformatics can superficially suggest SAM binding, but such proteins can in fact exhibit catalytic activities dramatically different from methyl transfer, such as, for example, oxidation and cycloaddition chemistry.[24–29] We, therefore, set our course to delete *dynO6* and *dynA5* and examine their consequences.

RESULTS AND DISCUSSION

CRISPR-cas9 was utilized[11] to remove *dynO6* from the *Micromonospora chersina* genome. Small-scale fermentation of the deletion mutant confirmed complete loss of DYN production and the accumulation of a single new product **10** at slightly longer HPLC retention times

and exhibiting a similar UV–vis absorption spectrum compared to DYN (Figure 2a,d,e). The mass spectrum predicted a molecular formula of $C_{29}H_{17}NO_8$, that is, a loss of CH_2O compared to DYN. To characterize the structure of **10**, a 12L fermentation of the Δ*dynO6* strain was supplemented with [1-^{13}C]- and [2-^{13}C]acetate to increase the sensitivity of NMR analyses. Acetylation of crude **10** to facilitate purification afforded the tetraacetate **10a,** indicating the presence of four hydroxyl groups, unlike the three in DYN (**1**) (Figure 2c).

It was immediately apparent from the ^{1}H NMR spectrum that the new metabolite lacked the −OCH_3 singlet present in DYN triacetate **11**, but the pattern of the A- and C-ring hydrogens, the characteristic N–H doublet (*δ*9.42, *J* = 4.2 Hz), and the four coupled hydrogens of the enediyne bridge spanning C2 and C7 were all little changed from DYN triacetate **11**. Resonances for three relatively downfield aryl *O*-acetyl methyls were clustered at *δ*2.46, 2.37, 2.33, and a fourth at *δ*2.31 was attributed to the enolacetate at C30. The complete ^{1}H- and ^{13}C-spectra of **10a** were assigned by chemical shift comparisons to DYN triacetate **11** and full HSQC and HMBC correlation spectroscopy (Figures S11 and S12, respectively). Especially telling, however, was the loss of the relatively labile enolacetate upon aqueous workup or silica gel chromatography. The resulting triacetate **10b** (Figure 2c) gave a distinctly altered ^{1}H NMR spectrum, in which the *β*-ketoaldehyde enol tautomer was exclusively observed with H30 at *δ*9.24 and the enol hydrogen dramatically deshielded at *δ*16.9 owing to its strong intramolecular hydrogen bond to the C6 ketone, securing the structure of the new metabolite **10**. The ^{13}C chemical shifts of C3 and C8 at 72.8 and 62.6 ppm, respectively, were close to those observed in DYN triacetate and confirmed the presence of the epoxide.

To demonstrate that ketoaldehyde **10** is an on-pathway intermediate of DYN biosynthesis, the peracetate of ^{13}C-enriched **10** was stirred with DMSO and water overnight to gently remove all acetate groups prior to administration to *M. chersina* without added NaI (to effectively eliminate de novo DYN biosynthesis).[16] Mass spectrometric analysis of the isolated DYN compared to that at natural abundance ^{13}C revealed that the incorporation of **10** was >90% (Figures 2b and S6).

Unlike the Δ*dynO6* mutant, deletion of *dynA5* from *M. chersina*, again using CRISPR-Cas9, did not fully eliminate DYN production, but decreased it to ~55%, accompanied by two new metabolites **12** and **13** (Figure 3a), whose structures were unambiguously determined by a combination of spectroscopic methods (Figures S13–S25) as above and briefly summarized in the following. The characterization of **12** and **13** proved troublesome owing to low titers in the Δ*dynA5* strain. Inspired by related work,[10] we overexpressed two genes predicted to be transcriptional activators, *dynR2* and *dynR7*, in the *dynA5* knockout mutant to generate Δ*dynA5_pSUE_R2/R7*. This new strain displayed >10-fold increased production of **12** and **13** along with DYN (**1**). Both **12** and **13** were isolated from an 18L fermentation supplemented with [1-^{13}C]- and [2-^{13}C]acetate to facilitate NMR characterization. Exact mass measurements of **12** and **13** yielded molecular formulae $C_{19}H_{20}NO_7$ and $C_{29}H_{20}NO_6$, respectively, whose UV–vis absorption spectra and those of DYN are shown in Figure 3c–e.

To ease further purification of **13**, its triacetate **13a** was prepared. Several features were soon apparent in the ^{1}H NMR spectrum. First, the diagnostic four-spin system of the enediyne

bridge in **10** above and DYN (**1**) was missing and replaced by a new four-spin system indicative of Bergman rearrangement to a C2–C7 bridging phenyl ring.[8] The N–H doublet (δ10.47, J = 4.2 Hz) was present deshielded by the proximal phenyl ring as well as the C-ring H10 singlet, albeit shifted ~0.5 ppm upfield compared to the triacetate of DYN **11** in keeping with the change in the nearby chemical environment. The three A-ring hydrogens matched those of metabolite **14** seen earlier in both chemical shift and mutual coupling constants.[8,11] and placed an acetoxy (hydroxy) group at C18 (Scheme 1).

In these prior experiments, two cytochromes P450 encoded in the DYN BGC, Orf19 and E10, were deleted pairwise to give **15** lacking the two DYN A-ring hydroxyls in undiminished yield. Individual knockouts of these genes assigned their functions specifically at C18 (Orf19) and C15 (E10) as late-stage tailoring modifications in DYN biosynthesis. The appearance of C18 hydroxylation in **12** and **13** is consistent with the previously observed preference or kinetic order, favoring C18 hydroxylation over C15.[11] That C18 hydroxylation is seen in both **12** and **13** appears out of order or synthetically premature, but it is a reminder that biosynthetic enzymes can exhibit considerable substrate flexibility, as exemplified particularly among the AFEs.[23,30] This behavior can be amplified in studies of blocked mutants, where true pathway intermediates, shunt products, and related co-metabolites accumulate in artificially elevated concentrations to undergo reaction and confound accurate substrate/precursor identification. A further indication of adventitious behavior is seen in the C7 oxidation of **12** to **13, which is** unrelated to the main pathway to DYN but could reflect parallel transformations in the biosynthesis of other AFEs **2**, **3**, and **4**. The identity of the enzyme responsible is not known.

The F-ring methyl (C29), which appears as a doublet in DYN, now gives a singlet at 1.65 ppm, consistent with attachment to an alkene. While puzzling at first, in accordance with its high oxidation state, only a single uncoupled hydrogen at δ3.81 and a weakly coupled pair of hydrogens (J = 1.6 Hz) of widely separated chemical shifts (δ3.59 and 5.26) remained unassigned. 2D-correlation to the carbon skeleton led directly to the structure of **13** (Figures 4 and S20–S25), highlighted by the striking connection between C5 and C30. By applying similar logic to **12**, the absence of the H7 singlet and the addition of oxygen to the molecular formula led quickly to the structure, which was underscored by the marked downfield shift (~25 ppm) of C7 owing to hydroxylation at this carbon (Figure 3).

To test for true methyltransferase function by DynO6 but not DynA5, [^{13}C-methyl]-L-methionine was administered to a fermentation of the Δ*dynA5_pSUE_R2/R7* strain. An approximately 30% specific incorporation of label was observed into the methoxy of the DYN produced, but no carbon enrichment was seen in either **12** or **13**, consistent with a non-methylase function of DynA5 in the biosynthesis but further verification of that late tailoring role by DynO6. The strong sequence and functional correlation of DynO6 to other *O*-methyltransferases coupled with the intact incorporation of **10** into DYN, established it as the required SAM-dependent *O*-methyltransferase in DYN biosynthesis to give a late intermediate of the pathway.

In keeping with early hydroxylation at C18, a compound identical to **12** but lacking this aryl oxidation has been observed in the course of a methodologically different

investigation of DYN/AFE biosynthesis, as will be discussed further below. But first, the Liang group reported a *Micromonospora* sp. MD118 that harbors a truncated enediyne BGC evolutionarily related to those that support DYN (**1**), UNC (**2**), TNM (**3**), and YPM (**4**, Figure 1) biosynthesis,[2,4–6,10] but lacks putative biosynthetic genes common to the latter AFE BGCs; that is, *dynE13, dynA1, dynA2, dynA4,* and *dynA5* (Figure S1 and Table S6). The MD118 strain does, however, encode the biosynthetic proteins sufficient to carry out the early pathway transformations including bifurcation to the enediyne arm of AFE synthesis and construction of the iodoanthracene-γ-thiolactone **8**, the key building block of the anthraquinone "half" of all AFEs.[16,31,32] The fermentation of MD118 yielded a family of products, the sungeidines A–H, in which presumed precursor enediyne products have undergone spontaneous Bergman cyclization to the corresponding bridging phenyl species observed. In the interest of space and to streamline the discussion that follows, only the structures of sungeidines B (**16**) and C (**17**) are shown below[10] The most important observation that could be made about all sungeidines A–H was that the site of iodination in **8** is directly connected to a nitrogen that ultimately appears in all AFEs. That is, the joining of the "upper" enediyne half and the "lower" anthracene/anthraquinone half involved aryl C–N bond formation.[9] A subsequent process would link C8 and C9 to complete the heterodimerization and lead to DYN and the other known AFEs.

At about the time of this report, we described the CRISPR-cas9 deletion of *dynE13* in wild-type *M. chersina*.[8] As noted above, this gene, while not present in MD118, is shared by the other AFEs 2, 3, and 4 (Figure S1).[10,32] The Δ*dynE13* mutant accumulated four principal products, each closely related in structure to the sungeidines, e.g., B (**16**) and C (**17**).[31] Again, to simplify the presentation, only **18** and **19** are shown from the Δ*dynE13* deletion mutant, where the latter interestingly retains its 10-membered enediyne (Scheme 2).[8] In addition, evidence was gathered that DynE13 is responsible for the oxidative conversion of the anthracene-δ-thiolactone **8** to the anthraquinone core of the AFEs at some point beyond the initial C–N coupling step[8] and not epoxidation, as suggested in the early interpretation of the DYN BGC.[6]

Returning to the structures of **12** and **13** isolated from the Δ*dynA5* mutant of *M. chersina*, Ma et al. carried out correlative experiments, in which MD118 served as the host for a series of gene-dosing studies, in which candidate DYN biosynthetic genes that have orthologs among the **1**, **2**, **3**, and **4** BGC's were examined for their additive effect on metabolite production. Of the many experiments described, one especially pertinent to the present discussion added back *dynE13, dynA1, dynA2,* and *dynA4*. Fully congruent with the isolation of **13** from the Δ*dynA5 M. chersina* deletion, the same product **25** without an A-ring hydroxyl group was synthesized (Scheme 3).

Each of the sungeidines A–H has a variously hydroxylated A-ring but is regiochemically distinct from DYN. Like the DYN producer *M. chersina,* MD118 also contains two cytochrome P450-encoding genes, *sgd19* and *sgdE10*.[31] As was done for Δ*dynorf19* and Δ*dynE10 M. chersina* strains,[11] the two MD118 P450 genes were deleted, and the resulting strain MD118AΔΔ was found to yield a narrower metabolite spectrum almost identical to that seen previously in the Δ*dynE13* deletion mutant in *M. chersina* described above.[8]

Importantly, the representative structures **18** and **19** shown above were now seen to be common to both investigations (Scheme 2).

The introduction of DynE13, the putative DYN flavin-dependent oxidoreductase, into the truncated host pathway as MD118AΔΔ::*dynE13* abolished all sungeidine synthesis but did not result in the appearance of any new metabolites. However, when another putative DYN biosynthetic gene was added, *dynA1*, to give the construct MD118AΔΔ::*dynE13*/*dynA1*, anthracene-γ-thiolactone products, also observed earlier in the Δ*dynE13* mutant of wild-type *M. chersina*, e.g., **18** and **19** (Scheme 2), were completely replaced by three anthraquinone-containing structures **20–22**[31] (Scheme 3) in accordance with the deductions about the role of DynE13 noted above.[8] The appearance of an amine in **22** might be thought to represent the unknown aryl C–N bond formation that initiates the heterodimerization. Recent experiments with synthetic aminoanthracene **23**, however, firmly established that it is not involved in DYN biosynthesis,[9] and indeed, studies reported in Ma et al. suggest that **22** is likely a degradation product arising from pathway intermediates or shunt products.[31] In the development of a unified mechanistic understanding of AFE biosynthesis and of DYN (**1**) in particular, structure **21** is most germane because when *dynA2* was co-expressed in MD118AΔΔ::*dynE13*/*A1*/*A2*, small amounts of **21** and **22** were again observed but dominated by the production of **24** (Scheme 3), in which the pivotal C8–C9 bond had formed to accomplish the second of the heterodimerization reactions that link the “upper” and “lower” halves of the AFEs. Both DynA1 and DynA2 show sequence similarity to the versatile SnoaL-like cyclase/hydroxylase/aldolase enzyme family.[33–35] How the critical C8–C9 bond actually forms is, however, controversial in the literature,[10,32] and will be taken up later below.

To bring the discussion back to the isolation of **12** and **13** (Figure 3) from the Δ*dynA5* deletion mutant of *M. chersina*, the effect of DynA4 was assessed by the Liang group in MD118AΔΔ::*dynE13/A1/A2/A4*. Now, **25** was determined to be the major product, accompanied by only a minor amount of **24** (Scheme 3). Thus, by reconstituting the DYN biosynthetic pathway through DynA4, the same congested octacyclic skeleton was generated as by blocking the function of DynA5 in wild-type *M. chersina*. DynA4 precedes DynA5 in the biosynthetic pathway.

The role of DynA5 was addressed similarly to DynA4 by Ma et al.[31] Further progression of the DYN biosynthetic pathway was attempted with MD118AΔΔ::*dynE13/A1/A2/A4/A5*. Against expectation, the introduction of *dynA5* elicited no change in the distribution of metabolites and only **24** and **25** appeared, as with the incremental addition of *dynA4*. However, when a sixth gene was added back, *dynA3*, the synthesis of **24** and **25** was replaced by four new metabolites illustrated below, with **26** and **27** being the major components and the closely related **28** and **29** in lesser amounts (Scheme 4). The signal features of **26–29** are the loss of C30 and the almost certain intermediacy of an epoxide at the ring-D/F fusion that has undergone opening to the vicinal C3/C8 diol identically present in each structure. Leaving aside the curious appearance of thiomethyl substitution in the bridging phenyl rings of **26** and **27**, the role of DynA3 is enigmatic. While *dynA3* is present in the DYN BGC, it is not conserved in the BGC’s of UCL (**2**), TNM (**3**), or YPM (**4**) where orthologs of *dynE13, A1, A2, A4,* and *dynA5* are all clearly present (Figure S1 and Table

S6). Moreover, the latter three AFEs and DYN (**1**) each contain the critical epoxide essential to their potent DNA-cleaving ability. In sum, it can be deduced that DynA5 is responsible for introducing the epoxide.

Toward a Biogenetic Path to Dynemicin A.

Comparing the common skeletons of **12**, **13,** and **25** to the β-ketoaldehyde **10**, the sole product accumulated by the Δ*dynO6* deletion mutant of wild-type *M. chersina* suggests immediately that the F-ring enol is generated by retro-aldol reaction, in which the C30 carbinol in the former migrates to become the remote aldehyde (**32** to **35** in Figure 5). Moreover, a transformation like this would account for the mysterious observation from early ^{13}C-acetate incorporation experiments, where both C5 and the C30 carboxylate of DYN arise from the C2 of acetate. For such a carbon migration to proceed, however, the retro-aldol requires an alternative electron sink. It was realized that, rather than trivial reversion of the aldol product to the F-ring C6 ketone, the electron-deficient anthraquinone **34** affords a highly delocalized electron sink, as depicted in Figure 5. The universal presence of the key epoxide in DYN (**1**), UCL (**2**), TNM (**3**), and YPM (**4**) implies common steps up to the creation of the epoxide ring. We propose its introduction is inextricably linked to the aldol/retro-aldol bond reorganizations to the highly electrophilic intermediate **36**. The core skeleton shared by **12**, **13**, and **25** is ideally suited to react, according to classical chemical precedents, as set out in Figure 5. The return of the electrons from the retro-aldol step terminates in protonation at C4 to set the F-ring methyl (C29) stereochemistry in **35** and transiently place the reactive anti-Bredt alkene at the D/F-ring junction in **36** and conjugate it to the anthraquinone. Vinylogous β-addition of peroxide, whether spontaneous in solution from dihydroanthraquinone oxidation or bound/sequestered in DynA5, initiates Weitz–Scheffer epoxidation[36] to directly generate the centrally important epoxide **37**, whose formation would otherwise be exceedingly difficult to rationalize. The presumably higher effective concentration of reactants in DynA5 could account for greater synthetic efficiency and a higher flux to epoxide products. Such thermodynamically favored redox behavior by hydroquinone/dihydroanthraquinone substrates to generate hydrogen peroxide is well precedented in the literature.[37–39] and is advanced here to rationalize the seemingly contradictory activity of the Δ*dynA5* mutant to both accumulate two new metabolites **12** and **13** and yet retain the ability to support DYN biosynthesis.

Critical Role of a Dihydroanthraquinone Intermediate.

TnmK1 is an α,β-hydrolase fold enzyme from the TNM (**3**) producer that the Shen group recently demonstrated catalyzes the key C8–C9 linkage,[32] the second step of heterodimerization, but in conflict with the results of Ma et al. recounted above.[31] Such a C–C bond-forming reaction is not otherwise known for this enzyme superfamily. Despite X-ray structures of TnmK1 with and without its substrate TNMH (**38**) bound and extensive mutagenesis experiments of presumed catalytic residues, it is not clear how C–C bond formation is mediated by TnmK1.[32] Nonetheless, a plausible mechanism was proposed as illustrated in Figure 6. Contra-thermodynamic tautomerization of the anthraquinone **38** to keto-imine **39** was invoked to enable Michael addition to the newly electrophilic C-ring and accommodate C8–C9 bond formation. Remarkably, the product TNM I (**40**) was isolated

and characterized in a state, where expected C-ring enolization and aromatization have not occurred. In vitro demonstration of this surprising transformation was also shown for recombinant UclK1 and DynA4, orthologs encoded by the UCL and DYN BGCs, respectively.[32]

It must also be noted that specific incorporation of the product TNM I (**40**) into tiancimycin A (**3**) or DYN (**1**), hence demonstration of biosynthetic intermediacy, was not demonstrated. Given that true intermediacy of the β-ketoaldehyde **10** in the biosynthesis of DYN was importantly established here, early *O*-methylation evident in TNM H and TNM I has the mechanistic consequence that both are incapable of the essential aldol/retro-aldol steps to migrate the bridgehead aldehyde in **32** to the F-ring and enable epoxidation (Figure 5). Further consideration of the structures of TNM H (**38**) and TNM I (**40**), but eliminating the *O*-methylation catalyzed in the TNM pathway, we arrive at structure **30** (Figure 5) and, by analogy to Figure 7, via **30** to **32**. The presence of the F-ring ketone is essential to make possible aldol closure to **33**, which may be facilitated by the relief of overall strain in the system by aromatization and planarization of the C-ring. With the re-formation of the electron-rich dihydroanthraquinone, aerial oxidation yields hydrogen peroxide and re-establishment of the thermodynamically favored anthraquinone core **34** (Figure 5). It can be readily seen that the Bergman rearrangement of the enediyne after epoxidation would give the bridging phenyl ring in cometabolites **12** and **13**.

Chemical Model Reactions.

Recognizing the synthetic potential of the Δ*dynA5* metabolites **12** and **13** as well as the shared core of the DynA4 reconstitution product **25** in MD1118AΔΔ stimulated the biogenetic proposal depicted in Figure 5. In vitro experiments with reconstituted DynA4 and homologues TnmK1 and UclK1 dictated that the direct product from **38** of these identically functioning enzymes is **40**, which is in the reduced dihydroanthraquinone oxidation state **32**/**33**. “Cofactor less” oxidations are precedented from hydroquinone substrates that naturally oxidize in air to generate hydrogen peroxide (H_2O_2) that further reacts with the resulting quinone/anthraquinone to generate oxidized products.[37–39] We elected to attempt chemical model reactions to mimic, and thus support, the chemical logic of the biogenetic steps embodied in Figure 5. Compounds **12a** and **13a** were separately reacted with 1 equiv of the urea $^{\bullet}H_2O_2$ complex and DBU[40] for each *O*-acetyl group in anticipation that each acetate would be removed by peroxide anion generated in situ, and the base would initiate retro-aldol reaction, in which the pre-existing anthraquinone would serve as the electron sink. Further electron movement to re-establish the anthraquinone core would place the starting alkene in conjugation at the D/F-ring fusion, and C4 protonation would place the methyl group (C29) on the β-face of the F-ring as naturally occurs in DYN (**1**) and **10**.

Reactions of **12a** and **13a** were carried out on a milligram scale in dry THF for 6 h at room temperature. In each instance, thin-layer chromatography showed the disappearance of the pinkish-orange starting material and the formation of a major bluish-purple product, a striking hue very like DYN (**1**). Owing to the limited amounts of **12a** and **13a** available, the reaction mixtures were concentrated in vacuo and directly purified by reverse-phase HPLC. The UV–vis spectra of the isolated products were virtually identical (Figure 7) and closely

resembled that for DYN. Electrospray ionization mass spectrometry (ESI-MS) analysis of the major product from each reaction gave molecular formulae of $C_{29}H_{19}NO_8$ from **12** and $C_{29}H_{19}NO_7$ from **13**, respectively, i.e., the products from both reactions revealed the addition of a single oxygen atom in keeping with either the formation of the hoped-for epoxide or oxidation of the F-ring aldehyde to a carboxylic acid and retention of the C3–C4 double bond in the F-ring.

As a larger amount of ^{13}C-enriched **12a** had been isolated, its reaction with hydrogen peroxide and base was examined in detail first. Immediately apparent in the ^{1}H NMR spectrum of the principal product **42** were two sharp, highly deshielded singlets at δ13.66 and δ12.98 for the strongly hydrogen-bonded anthraquinone *peri*-hydroxy groups at C18 and C11. This feature signified that the hydroxy/aminoanthraquinone core remained intact in the product, in keeping with its characteristic UV–vis signature and molecular mass. The diagnostic N–H doublet (J = 4.2 Hz) was seen at δ10.74, very close to its chemical shift in both **12a** and **13a**, deshielded compared to the enediynes **1** and **10** by the bridging (C2–C7) phenyl ring. Its coupling partner H2 appeared at δ5.24, no longer allylic to the C3–C4 double bond present in the starting material and shifted ~0.5 ppm upfield in line with the behavior of H2 in the epoxide-containing Δ*dynO6* product **10**. Moreover, the C29 F-ring methyl group appeared as a doublet at δ1.51 coupled to H4, which appears as a quartet (J = 7.2 Hz) and unambiguously eliminated the possible presence of a double bond at C4 (δ39.5). The important H30 hydrogen of the enolized F-ring aldehyde was observed at 8.02 ppm, in excellent agreement with the Δ*dynO6* metabolite **10** at 8.09 ppm. Further direct and long-range H/C-correlations were carried out by COSY, TOCSY, and HMBC measurements (Figures S26–S30). Notably, epoxide carbons were identified at δ72.4 and δ58.9 and the F-ring ketone at δ197.8 correlating well with the corresponding resonances in **10**. In sum, these structural comparisons showed that 1D- and 2D-NMR data led directly to structure **42** and, by applying identical logic, to **43** (Figures S31–S34). Finally, only one inconsistent observation was made in the course of these NMR analyses. In both **42** and **43,** the H4 quartet appears at δ3.26, whereas the closest comparison would be made to enediyne **10,** where this hydrogen appears at δ3.96. As a consequence of the relative upfield shift (~0.7 ppm) of H4 in **42** and **43**, it was assigned the configuration opposite to that of the natural products and resided in the shielding cone of the bridging phenyl ring. In an attempt to confirm this absolute configuration at C4, a ROESY analysis was run. While a clear correlation was observed between H4 and its geminal C29 methyl, no proximal interaction between H2 and either H4 or the C29 methyl group could be detected (Figure S30). As the magnitude of this through-space effect varies with the inverse sixth power of distance, unfortunately, no information was provided to discriminate between the two possible H4 orientations. We attribute this single stereochemical difference between the native biosynthesis and the chemical model reactions to be caused by the presence of either a C2–C7 bridging enediyne, as in **10** and in the proposed intermediate **35** (Figure 5), or a phenyl ring as in **12** and **13** used in the chemical model reactions. The latter would constrict the conformational flexibility of the D,E,F-rings and reverse the course of C4 protonation in **42** and **43**.

CONCLUSIONS

Of the three identified structural types of enediyne antitumor antibiotics, the anthraquinone-fused enediynes (AFEs) are distinguished by the central linkage of two halves derived from an iodoanthracene-γ-thiolactone **8** and an aminoenediyne coupling partner **9** (Figure 1b), whose structure is not fully known. Some details of the unusual aryl C–N bond-forming step have been reported recently,[9] as have experiments to identify subsequent catalysis of the C8–C9 bond necessary to complete heterodimerization and bring the "upper" and "lower" halves together.[31,32] Between these two pivotal biosynthetic events, a flavin-dependent dehydrogenase, DynE13, and its orthologs in other AFE biosynthetic pathways intervene to oxidize the anthracene-γ-thiolactone to the C-ring hydroxylated anthraquinone present in TNM H (**38**), TNM I (**40**) **9**, **10**, and **7** and are common to all naturally occurring AFEs.[8,10]

There is disagreement in the literature about how the critical C8–C9 bond is formed. First, the results of Gui et al.[32] give evidence that TnmK1 (and homologs UclK1 and DynA4) mediates this process. On the other hand, the sequential introduction of biosynthetic genes from the DYN BGC into MD118AΔΔ, which has only the early genes needed for AFE biosynthesis, assigns this important C–C bond-forming reaction to DynA2.[31] Second, one of the conclusions from the Liang group's work and ours is that the product of DynA4 is the aldol product **25**, which itself would be observed as the trivial but thermodynamically favored oxidation product of initially formed dihydroanthraquinone **33** and by blocking the function of DynA5 (Figure 5). Third, both **38** and **40** are said to be intermediates in AFE biosynthesis.[32] Unfortunately, no experimental verification of intact incorporation into either TMN or DYN was reported. As **38** accumulated in a blocked mutant in the TNM pathway, it is possible that an ordinarily late tailoring reaction like *O*-methylation has taken place to divert a true intermediate. The work of the Shen laboratory and others has documented just how promiscuous *O*-methylases as well as cytochromes P450 in AFE biosynthesis can be.[11,30] More fundamentally, the *O*-methylation evident in **38** and **40** would prohibit the aldol closure reaction from occurring to the DynA4 product **33** and require the F-ring C6 ketone (Figure 5). In the absence of proof of intermediacy of **38** or **40**, a demethylation event would have to be invoked to generate the aldol products. Such enzyme-mediated processes are known but lack bioinformatic or experimental support in this instance. Fifth, genetic complementation of the *tnmK1* knockout restored synthesis of TNM (**3**) as anticipated but also gave rise to a co-metabolite **41** (see above)[32] bearing striking structural similarity to **26–29** and having the same elevated oxidation state observed by the Liang laboratory in their pathway "retrofitting" experiments upon the inclusion of *dynA5*.[31] It is fortunate that both **12** and **13** are isolated as stable anthraquinones poised to undergo the proposed retro-aldol reaction to migrate the C30 carbinol to become the F-ring aldehyde seen in **10**. Despite spontaneous Bergman rearrangement having already occurred, remarkably facile and selective retro-aldol scission takes place in the presence of the urea•hydrogen peroxide complex and DBU. Subsequent conjugate addition of peroxide and ensuing epoxide formation are synthetically well precedented in the work of Julia and Colonna[40] and give compelling evidence in support of the biogenetic proposal set out in Figure 5. As an aside, it is instructive to compare and contrast this synthetic strategy, where the strained enediyne is already in place before epoxide formation takes place, with

that adopted in total chemical syntheses of DYN, where a *cis*-fused ring-D/F precursor is enforced by epoxidation to draw C3 and C7 sufficiently close to enable the bridging enediyne to be successfully introduced.[41–43]

The salient vicinal diol at the ring D/F junction is common to **26–29**, and **41** derives from the opening of the C3–C8 epoxide that we propose is introduced in a Weitz–Scheffer reaction. The migration of C30 as a consequence of the aldol/retro-aldol sequence invoked in Figure 5 would place C30 as an aldehyde at C5 in the F-ring, as shown. The absence of C30 and the presence of a hydroxyl at C5 (and by enediol isomerization to C6) in **26**/**27** (and **28**/**29**) could be accounted for in a Baeyer–Villiger oxidation at C30 or by elevation of C30 to a carboxylic acid, which natively occurs late in the biosynthesis of DYN, followed by decarboxylation of the resulting β-ketoacid and final hydroxylation at C5. Dehydration of this alcohol would give rise to the C4/5 double bond seen in **41**. Such processes would also account for the absence of C30 in other AFEs.

It is certainly true that the F-ring is partially destroyed in **2**, **3**, and **4** compared to DYN. Those processes are likely oxidative, as intimated by **26–29** and **41**. While available evidence suggests that this hypothesis could be true, direct proof cannot be claimed at present. Stable late intermediates like **10** from the *dynO6* deletion mutant might be tested for their possible intermediacy in other AFE biosynthetic pathways where the F-ring is substantially modified from that of DYN. These questions remain objects of further investigation and validation.

EXPERIMENTAL SECTION

Gene Deletion Using CRISPR-Cas9.

CRISPR-Cas9 plasmids with homologous recombination templates and sgRNAs were electroporated into *Escherichia coli* GM2929 *hsd*S::Tn10 (pUB307::Tn7) and cultured to transfer to *M. chersina* by conjugation, as previously described.[11,44] The resulting spore/*E. coli* mixture was plated on medium 53 with 2% agar plates supplemented with 10 mM $MgCl_2$. The plates were incubated at 28 °C overnight. Afterward, nalidixic acid and apramycin in sterile ddH_2O (20 and 50 μg/mL, respectively) were overlaid on the plates. The plates were then incubated at 28 °C for 7 days.

The ex-conjugates were restreaked three times: first on to medium 53 agar plates with nalidixic acid and apramyicin; next on medium 53 agar with nalidixic acid, apramycin, and thiostrepton (1 μg/mL) plates to induce the CRISPR-Cas9; and lastly on medium 53 agar plates without drug to recover. After each restreak, the plates were incubated at 28 °C for 7 days. Mutants were finally screened by colony PCR, and gene deletions were confirmed by isolation, PCR, and sequencing of the gDNA.[11]

Construction of the pSUE Plasmids.

Using the genomic DNA of *M. chersina* as a template, *dynR2* and *dynR7* were PCR amplified. In order for the genes to be unidirectional and adjacent, the *dynR2* R primer had an overlapping region with *dynR7* F. To combat the difficulties associated with a GC-rich sequence, Phusion High-Fidelity DNA polymerase, GC-rich buffer, and 10% (v/v)

DMSO were added to the Gibson Assembly reactions. The PCR products were assembled into a EcoRV and BamHI-digested pSUE plasmid to yield pSUE_*dynR2/R7*. The plasmid was then transformed into Subcloning Efficiency DH5α Competent Cells (Thermo Fisher Scientific). Selection of colonies was done after growth on apramycin (50 μg/mL)/LB agar at 37 °C overnight and a restriction enzyme screening. Positive clones were grown overnight in LB and 50 μg/mL apramycin. Plasmids were isolated using a GeneJET Plasmid Miniprep Kit (Thermo Fisher Scientific) and then sequenced.

Incorporating the pSUE Plasmid into the *M. chersina* Genome.

The pSUE plasmids were conjugated into electrocompetent cells, *E. coli* GM2929 *hsd*S::Tn10 (pUB307::Tn7). The conjugation protocol into *M. chersina* was the same as that used to introduce gene deletions with CRISPR-Cas9, as above and as described previously.[9]

Ex-conjugates were restreaked two times: once on to medium 53 agar with nalidixic acid and apramyicin for selection, and lastly on medium 53 agar without drug to recover from the antibiotic selections. After each restreak, the plates were incubated at 28 °C for 7 days.

Small-Scale Fermentation of Δ*dynO6* and Δ*dynA5* Mutants.

100 μL of the mycelial stocks of CRISPR-Cas9 mutants, 10 μL of spores of wild-type *M. chersina*, and 10 μL of DynE8 (PKS knockout mutant strain) were plated on medium 53 with 2% agar plates and incubated for 7 days at 28 °C. The resulting mycelia were used to inoculate 50 mL of medium 53 in 125 mL shake flasks with ~3.0 grams of sterile glass beads (0.2 mm in diameter). The cultures were incubated at 28 °C at 250 rpm for 7 days. Afterward, 2 mL of the vegetative cultures were used to inoculate 50 mL of H881 cultures in 250 mL flasks, which were fermented at 28 °C for 7 days. On the third day, 1% (w/v) sterile Diaion HP-20 resin was added to each fermentation.

HPLC Analysis of Metabolites in the Δ*dynO6* and Δ*dynA5* Mutants.

5 mL of each day-seven fermentation broth was extracted with an equal volume of ethyl acetate (EtOAc). Extracts were centrifuged at 4000*g* for 10 min at 4 °C. 4 mL of the EtOAc layer was taken up and put on a SpeedVac to dry without heating. The dried extract was resuspended in 200 μL DMSO and filtered through 0.2 μm polytetrafluoroethylene (PTFE) filters. 75 μL of each sample was analyzed by an Agilent 1200 HPLC equipped with a Prodigy ODS3 100 A, 5 μm, 250 × 4.6 mm column (Phenomenex). A gradient method from 5 to 95% ACN + 0.1% (v/v) formic acid over 40 min (with a 10 hold at 95% ACN before column re-equilibration) with a 1 mL per min flow rate was used to separate the products. The production of biosynthetic intermediates was monitored mainly at 280, 450, and 570 nm.

UPLC–ESI-MS Analysis of Compounds in the Δ*dynO6* and Δ*dynA5* Mutants.

For UPLC–ESI-MS analysis of metabolites, a 50 mL day 7 fermentation culture was extracted as described above. The concentrated EtOAc layer was resuspended in 2.5 mL of MeOH and filtered through a 0.2 μm polytetrafluoroethylene (PTFE) filter. The extract was analyzed on an Agilent 1100 HPLC using a Kinetex 100 Å, 5 μm, 250 × 10.0 mm C18 LC column (Phenomenex). Injections of 400–500 μL were separated using a gradient method

of 50–95% ACN + 0.1% (v/v) formic acid over 20 min, followed by a 5 min hold at 95% ACN before column re-equilibration (4 mL min^{-1} flow rate). Production of the metabolites was monitored at 280, 450, and 570 nm. Peaks were manually collected, frozen at −80 °C, and lyophilized. Lyophilized samples were re-dissolved in 200 μL MeOH and analyzed on a Waters ACQUITY/Xevo G-2 UPLC–ESI-MS with positive mode ESI ionization.

Chemical Model Reaction.[40]

Compounds **9a** (1.2 mg, 1.93 μmol) and **10a** (1 mg, 1.65 μmol) were separately dissolved in 2 mL of dry THF. DBU (1 M in THF) (7.72 μL, 7.72 μmol and 6.60 μL, 6.60 μmol, respectively) and urea-H_2O_2 (0.7 mg, 7.72 μmol and 0.6 mg, 6.60 μmol, respectively) were added sequentially to the above solution and left to stir under Ar for 6 h at room temperature. After completion of the reaction, the solvent was removed in vacuo, redissolved in DMSO, filtered through 0.2 μm PTFE filters, and analyzed on an Agilent 1200 HPLC using a Prodigy ODS3 100 Å, 5 μM, 250 × 4.6 mm column (Phenomenex). A gradient method of 5–95% ACN + 0.1% (v/v) formic acid over 40 min, followed by a 10 min hold at 95% ACN before column re-equilibration was used at a 1 mL/min flow rate to achieve separation of metabolites. Production of new products was monitored at 570 nm. The products were purified by 1100 Agilent HPLC equipped with a Luna 100 Å, 10 μm, 250 × 21.2 mm C18 LC column (Phenomenex). Injections of 400–500 μL were separated using a gradient from 20 to 95% ACN + 0.1% (v/v) formic acid over 50 min and a hold at 95% ACN for 10 min before column re-equilibration with a 4 mL per min flow rate. Each peak fraction was analyzed by UPLC–ESI-MS to identify the product of interest (Table S2). UPLC–ESI-MS $[M + H]^+$: calcd for **42** ($C_{29}H_{20}NO_8^+$), 510.1176; found, 510.1183; calcd for **43** ($C_{29}H_{20}NO_7^+$), 494.1234; found, 494.1233.

Supplementary Material

Refer to Web version on PubMed Central for supplementary material.

ACKNOWLEDGMENTS

The authors are deeply grateful to A. Majumdar (Director, Biophysical NMR Center, JHU) for help with NMR acquisition, I. P. Mortimer (Manager, Mass Spectrometry Facility, Department of Chemistry, JHU) for UPLC-MS support, and D. R. Cohen for helpful guidance and discussions. This work was supported by the NIH grant RO1 ES001670.

REFERENCES

(1). Konishi M; Ohkuma H; Matsumoto K; Tsuno T; Kamei H; Miyaki T; Oki T; Kawaguchi H; Vanduyne GD; Clardy J Dynemicin A, a novel antibiotic with the anthraquinone and 1,5-diyn-3-ene subunit. J. Antibiot 1989, 42, 1449–1452.

(2). Davies J; Wang H; Taylor T; Warabi K; Huang XH; Andersen RJ Uncialamycin, a New Enediyne Antibiotic. Org. Lett 2005, 7, 5233–5236. [PubMed: 16268546]

(3). Yan X; Ge H; Huang T; Hindra; Yang D; Teng Q; Crnovčić I; Li X; Rudolf JD; Lohman JR; Gansemans Y; Zhu X Huang Y; Zhao LX; Jiang Y; van Nieuwerburgh F; Rader C; Duan Y; Shen B Strain Prioritization and Genome Mining for Enediyne Natural Products. mBio 2016, 7, No. e02104. [PubMed: 27999165]

(4). Yan X; Chen JJ; Adhikari A; Yang D; Crnovcic I; Wang N; Chang CY; Rader C; Shen B Genome Mining of Micromonospora Yangpuensis DSM 45577 as a Producer of an Anthraquinone-Fused Enediyne. Org. Lett 2017, 19, 6192–6195. [PubMed: 29086572]

(5). Yan X; Chen JJ; Adhikari A; Teijaro CN; Ge H; Crnovcic I; Chang CY; Annaval T; Yang D; Rader C; Shen B Comparative Studies of the Biosynthetic Gene Clusters for Anthraquinone-Fused Enediynes Shedding Light into the Tailoring Steps of Tiancimycin Biosynthesis. Org. Lett 2018, 20, 5918–5921. [PubMed: 30212211]

(6). Gao Q; Thorson JS The Biosynthetic Genes Encoding for the Production of the Dynemicin Enediyne Core in Micromonospora Chersina ATCC53710. FEMS Microbiol. Lett 2008, 282, 105–114. [PubMed: 18328078]

(7). Tokiwa Y; Miyoshi-Saitoh M; Kobayashi H; Sunaga R; Konishi M; Oki T; Iwasaki S Biosynthesis of dynemicin A, a 3-ene-1,5-diyne antitumor antibiotic. J. Am. Chem. Soc 1992, 114, 4107–4110.

(8). Cohen DR; Townsend CA C–N-Coupled Metabolites Yield Insights into Dynemicin A Biosynthesis. ChemBioChem 2020, 21, 2137–2142. [PubMed: 32198800]

(9). Pal P; Alley JR; Townsend CA Examining Heterodimerization by Aryl C-N Coupling in Dynemicin Biosynthesis. ACS Chem. Biol 2023, 18, 304–314. [PubMed: 36696117]

(10). Low ZJ; Ma G-L; Tran HT; Zou Y; Xiong J; Pang L; Nuryyeva S; Ye H; Hu J-F; Houk N; Liang ZX Sungeidines from a Non-Canonical Enediyne Biosynthetic Pathway. J. Am. Chem. Soc 2020, 142, 1673–1679. [PubMed: 31922407]

(11). Cohen DR; Townsend CA A Dual Role for a Polyketide Synthase in Dynemicin Enediyne and Anthraquinone Biosynthesis. Nat. Chem 2018, 10, 231–236. [PubMed: 29359752]

(12). Thorson JS; Shen B; Whitwam RE; Liu W; Li Y; Ahlert J Enediyne Biosynthesis and Self-Resistance: A Progress Report. Bioorg. Chem 1999, 27, 172–188.

(13). Horsman GP; Chen Y; Thorson JS; Shen B Polyketide Synthase Chemistry Does Not Direct Biosynthetic Divergence between 9- and 10-Membered Enediynes. Proc. Natl. Acad. Sci. U.S.A 2010, 107, 11331–11335. [PubMed: 20534556]

(14). Bhardwaj M; Cui Z; Hankore ED; Moonschi FH; Esfahani HS; Kalkreuter E; Gui C; Yang D; Phillips GN; Thorson JS; Shen B; Van Lanen SG A Discrete Intermediate for the Biosynthesis of Both the Enediyne Core and the Anthraquinone Moiety of Enediyne Natural Products. Proc. Natl. Acad. Sci. U.S.A 2023, 120, No. e2220468120. [PubMed: 36802426]

(15). Belecki K; Townsend CA Biochemical Determination of Enzyme-Bound Metabolites: Preferential Accumulation of a Programmed Octaketide on the Enediyne Polyketide Synthase CalE8. J. Am. Chem. Soc 2013, 135, 14339–14348. [PubMed: 24041368]

(16). Cohen DR; Townsend CA Characterization of an Anthracene Intermediate in Dynemicin Biosynthesis. Angew. Chem., Int. Ed 2018, 57, 5650–5654.

(17). Singh S; Nandurkar NS; Thorson JS Characterization of the Calicheamicin Orsellinate C2-O-Methyltransferase CalO6. ChemBioChem 2014, 15, 1418–1421. [PubMed: 24978950]

(18). Kagan RM; Clarke S Widespread Occurrence of Three Sequence Motifs in Diverse S-Adenosylmethionine-Dependent Methyltransferases Suggests a Common Structure for These Enzymes. Arch. Biochem. Biophys 1994, 310, 417–427. [PubMed: 8179327]

(19). Singh S; Chang A; Goff RD; Bingman CA; Gruschow S; Sherman DH; Phillips GN; Thorson JS Structural characterization of the mitomycin 7-O-methyltransferase. Proteins 2011, 79, 2181–2188. [PubMed: 21538548]

(20). Abdelraheem E; Thair B; Varela RF; Jockmann E; Popadić D; Hailes HC; Ward JM; Iribarren AM; Lewkowicz ES; Andexer JN; Hagedoorn PL; Hanefeld U Methyltransferases: Functions and Applications. ChemBioChem 2022, 23, 1–19.

(21). Liscombe DK; Louie GV; Noel JP Architectures, Mechanisms and Molecular Evolution of Natural Product Methyltransferases. Nat. Prod. Rep 2012, 29, 1238–1250. [PubMed: 22850796]

(22). Jumper J; Evans R; Pritzel A; Green T; Figurnov M; Ronneberger O; Tunyasuvunakool K; Bates R; Žídek A; Potapenko A; Bridgland A; Meyer C; Kohl SAA; Ballard AJ; Cowie A; Romera-Paredes B; Nikolov S; Jain R; Adler J; Back T; Petersen S; Reiman D; Clancy E; Zielinski M; Steinegger M; Pacholska M; Berghammer T; Bodenstein S; Silver D; Vinyals O;

Senior AW; Kavukcuoglu K; Kohli P; Hassabis D; Hassabis D Highly Accurate Protein Structure Prediction with AlphaFold. Nature 2021, 596, 583–589. [PubMed: 34265844]

(23). Adhikari A; Teijaro CN; Yan X; Chang CY; Gui C; Liu YC; Crnovcic I; Yang D; Annaval T; Rader C; Shen B Characterization of TnmH as an O-Methyltransferase Revealing Insights into Tiancimycin Biosynthesis and Enabling a Biocatalytic Strategy to Prepare Antibody-Tiancimycin Conjugates. J. Med. Chem 2020, 63, 8432–8441. [PubMed: 32658465]

(24). Awakawa T; Zhang L; Wakimoto T; Hoshino S; Mori T; Ito T; Ishikawa J; Tanner ME; Abe I A Methyltransferase Initiates Terpene Cyclization in Teleocidin B Biosynthesis. J. Am. Chem. Soc 2014, 136, 9910–9913. [PubMed: 24992358]

(25). Fage CD; Isiorho EA; Liu Y; Wagner DT; Liu HW; Keatinge-Clay AT The Structure of SpnF, a Standalone Enzyme That Catalyzes [4 + 2] Cycloaddition. Nat. Chem. Biol 2015, 11, 256–258. [PubMed: 25730549]

(26). Cai Y; Hai Y; Ohashi M; Jamieson CS; Garcia-Borras M; Houk KN; Zhou J; Tang Y Structural Basis for Stereoselective Dehydration and Hydrogen-Bonding Catalysis by the SAM-Dependent Pericyclase LepI. Nat. Chem 2019, 11, 812–820. [PubMed: 31332284]

(27). Kim HJ; Ruszczycky MW; Choi SH; Liu YN; Liu HW Enzyme-Catalysed [4+2] Cycloaddition Is a Key Step in the Biosynthesis of Spinosyn A. Nature 2011, 473, 109–112. [PubMed: 21544146]

(28). Ohashi M; Liu F; Hai Y; Chen M; Tang M-C; Yang Z; Sato M; Watanabe K; Houk KN; Tang Y SAM-Dependent Enzyme-Catalysed Pericyclic Reactions in Natural Product Biosynthesis. Nature 2017, 549, 502–506. [PubMed: 28902839]

(29). Grocholski T; Dinis P; Niiranen L; Niemi J; Metsä-Ketelä M Divergent Evolution of an Atypical S-Adenosyl-L-Methionine-Dependent Monooxygenase Involved in Anthracycline Biosynthesis. Proc. Natl. Acad. Sci. U.S.A 2015, 112, 9866–9871. [PubMed: 26216966]

(30). Yang D; Ye F; Teijaro CN; Hwang D; Annaval T; Adhikari A; Li G; Yan X; Gui C; Rader C; Shen B Functional Characterization of Cytochrome P450 Hydroxylase YpmL in Yangpumicin A Biosynthesis and Its Application for Anthraquinone-Fused Enediyne Structural Diversification. Org. Lett 2022, 24, 1219–1223. [PubMed: 35084871]

(31). Ma G-L; Tran HT; Low ZJ; Candra H; Pang LM; Cheang QW; Fang M; Liang Z-X Pathway Retrofitting Yields Insights into the Biosynthesis of Anthraquinone-Fused Enediynes. J. Am. Chem. Soc 2021, 143, 11500–11509. [PubMed: 34293863]

(32). Gui C; Kalkreuter E; Liu YC; Adhikari A; Teijaro CN; Yang D; Chang C; Shen B Intramolecular C-C Bond Formation Links Anthraquinone and Enediyne Scaffolds in Tiancimycin Biosynthesis. J. Am. Chem. Soc 2022, 144, 20452–20462. [PubMed: 36279548]

(33). Sultana A; Kallio P; Jansson A; Wang JS; Niemi J; Mäntsälä P; Schneider G Structure of the Polyketide Cyclase SnoaL Reveals a Novel Mechanism for Enzymatic Aldol Condensation. EMBO J. 2004, 23, 1911–1921. [PubMed: 15071504]

(34). Kallio P; Sultana A; Niemi J; Mäntsälä P; Schneider G Crystal Structure of the Polyketide Cyclase AknH with Bound Substrate and Product Analogue: Implications for Catalytic Mechanism and Product Stereoselectivity. J. Mol. Biol 2006, 357, 210–220. [PubMed: 16414075]

(35). Beinker P; Lohkamp B; Peltonen T; Niemi J; Mäntsälä P; Schneider G Crystal Structures of SnoaL2 and AclR: Two Putative Hydroxylases in the Biosynthesis of Aromatic Polyketide Antibiotics. J. Mol. Biol 2006, 359, 728–740. [PubMed: 16650858]

(36). Weitz E; Scheffer A Über Die Einwirkung von Alkalischem Wasserstoffsuperoxyd Auf Ungesättigte Verbindungen. Chem. Ber 1921, 54, 2327–2344.

(37). Grocholski T; Koskiniemi H; Lindqvist Y, Mäntsälä P; Niemi J; Schneider G. Crystal Structure of the Cofactor-Independent Monooxygenase SnoaB from Streptomyces Nogalater: Implications for the Reaction Mechanism. Biochemistry 2010, 49, 934–944. [PubMed: 20052967]

(38). Siitonen V; Blauenburg B; Kallio P; Mäntsälä P; Metsä-Ketelä M Discovery of a Two-Component Monooxygenase SnoaW/SnoaL2 Involved in Nogalamycin Biosynthesis. Chem. Biol 2012, 19, 638–646. [PubMed: 22633415]

(39). Thierbach S, Bui N; Zapp J; Chhabra SR; Kappl R; Fetzner S Substrate-Assisted O2 Activation in a Cofactor-Independent Dioxygenase. Chem. Biol 2014, 21, 217–225. [PubMed: 24388758]

(40). Allen JV; Bergeron S; Griffiths MJ, Mukherjee S; Roberts SM, Williamson NM; Wu LE Juliá-Colonna Asymmetric Epoxidation Reactions under Non-Aqueous Conditions: Rapid, Highly Regio- and Stereo-Selective Transformations Using a Cheap, Recyclable Catalyst. J. Chem. Soc., Perkin Trans 1 1998, 3171–3180.

(41). Myers AG, Fraley ME; Tom NJ; Cohen SB; Madar DJ Synthesis of (+)-Dynemicin A and Analogs of Wide Structural Variability: Establishment of the Absolute Configuration of Natural Dynemicin A. Chem. Biol 1995, 2, 33–43. [PubMed: 9383401]

(42). Shair MD; Yoon TY, Mosny KK, Chou TC, Danishefsky SJ The Total Synthesis of Dynemicin A Leading to Development of a Fully Contained Bioreductively Activated Enediyne Prodrug. J. Am. Chem. Soc 1996, 118, 9509–9525.

(43). Nicolaou KC, Das D; Lu Y, Rout S; Pitsinos EN; Lyssikatos J; Schammel A; Sandoval J; Hammond M; Aujay M; Gavrilyuk J Total Synthesis and Biological Evaluation of Tiancimycins A and B, Yangpumicin A, and Related Anthraqui-none-Fused Enediyne Antitumor Antibiotics. J. Am. Chem. Soc 2020, 142, 2549–2561. [PubMed: 31976660]

(44). Kieser T; Bibb MJ; Buttner MJ; Chater KF; Hopwood DA Practical Streptomyces Genetics, John Innes Foundation: Norwich, 2000.

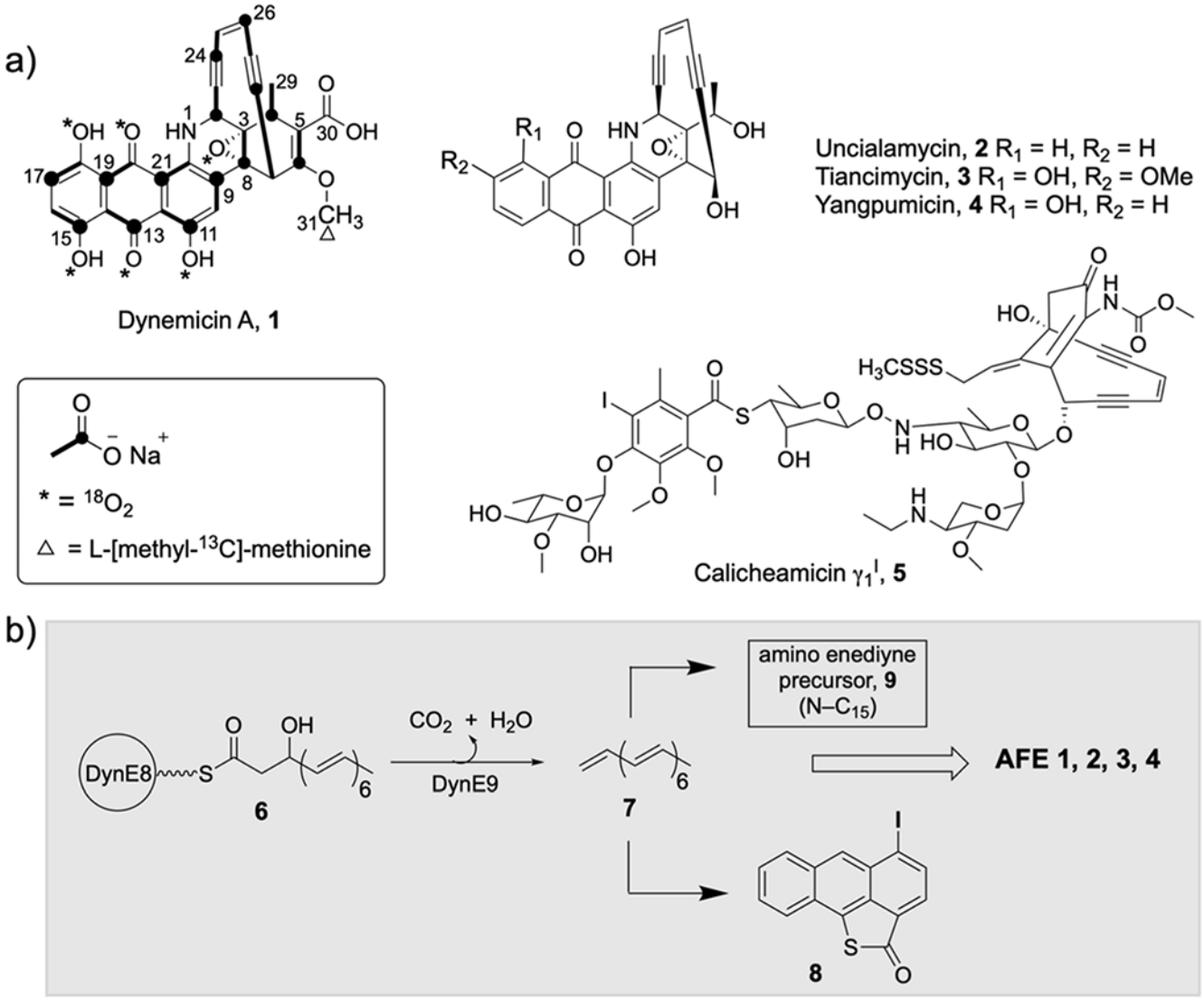

Figure 1.

(a) Structures of DYN (**1**) and closely related AFEs uncialamycin (UCL, **2**), tiancimycin (TNM, **3**), yangpumicin YPM, (**4**) and non-AFE calicheamicin (CLM, **5**). The acetate-labeling pattern of DYN is shown as a dot and bold-line representation, where the dot represents C1 of acetate and the bold-line represents the intact acetate unit. The triangle (Δ) represents carbon derived from L-[^{13}C-methyl]-methionine. The asterisks (*) denote the oxygen atoms derived from molecular oxygen. (b) Early biosynthetic steps shared by all AFEs.

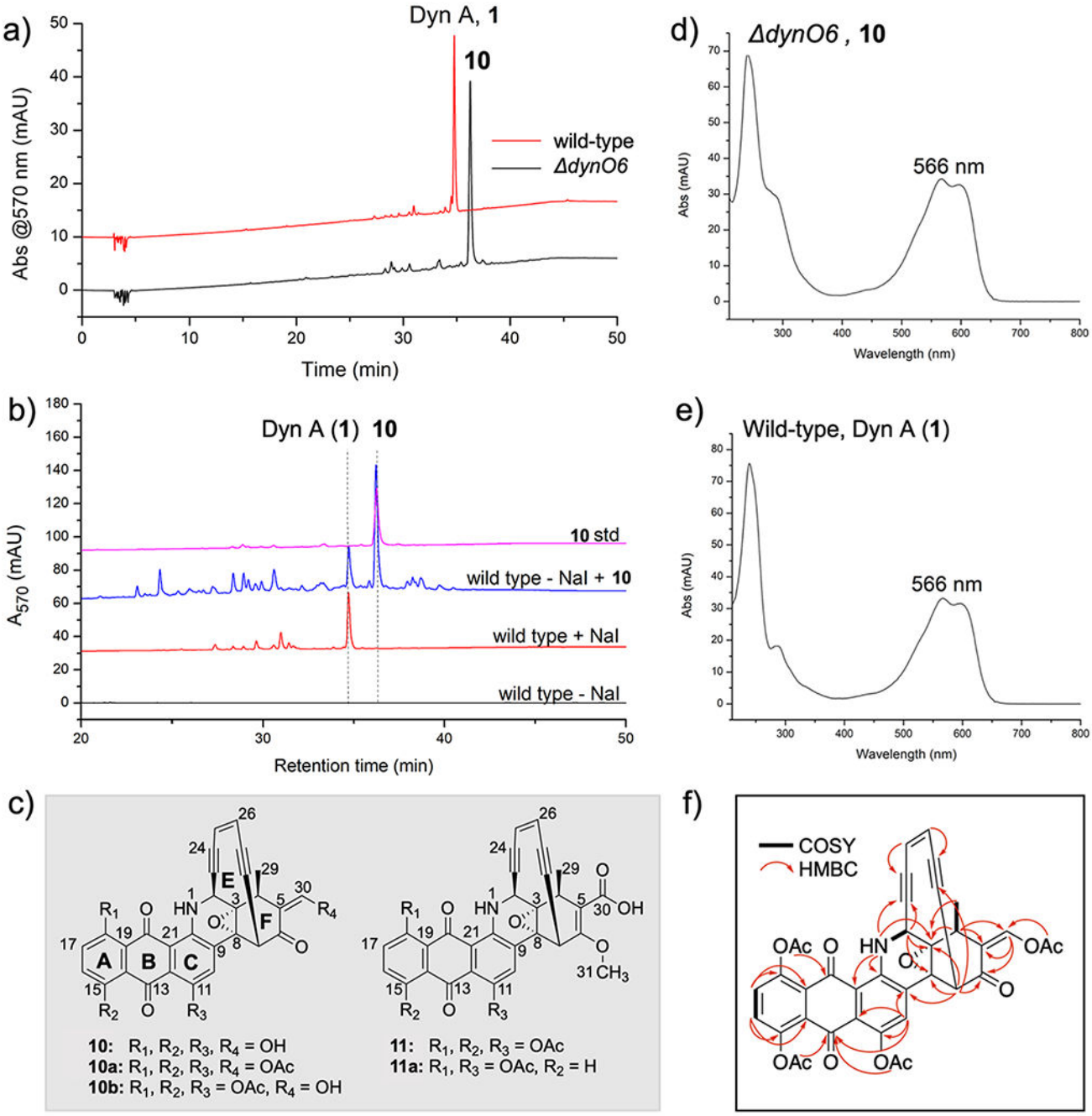

Figure 2.

Comparison of metabolites produced by wild-type *M. chersina* and Δ*dynO6*. (a) HPLC chromatograms at 570 nm demonstrating the loss of Dyn (**1**) production in the Δ*dynO6* mutant strain and accumulation of the *β*-ketoaldehyde **10** (b) restoration of DYN (**1**) production by **10** in wild-type *M. chersina* in the absence of added NaI with (c) the indicated structure of **10** along with the structures of acetylated dynemicins **11** and **11a** for structural comparison. (d) UV–visible spectrum of **10**. (e) UV–visible spectrum of DYN (**1**). (f) Key

NMR correlations used to solve the structure of **10a**, COSY, and HSQC spectroscopy as indicated.

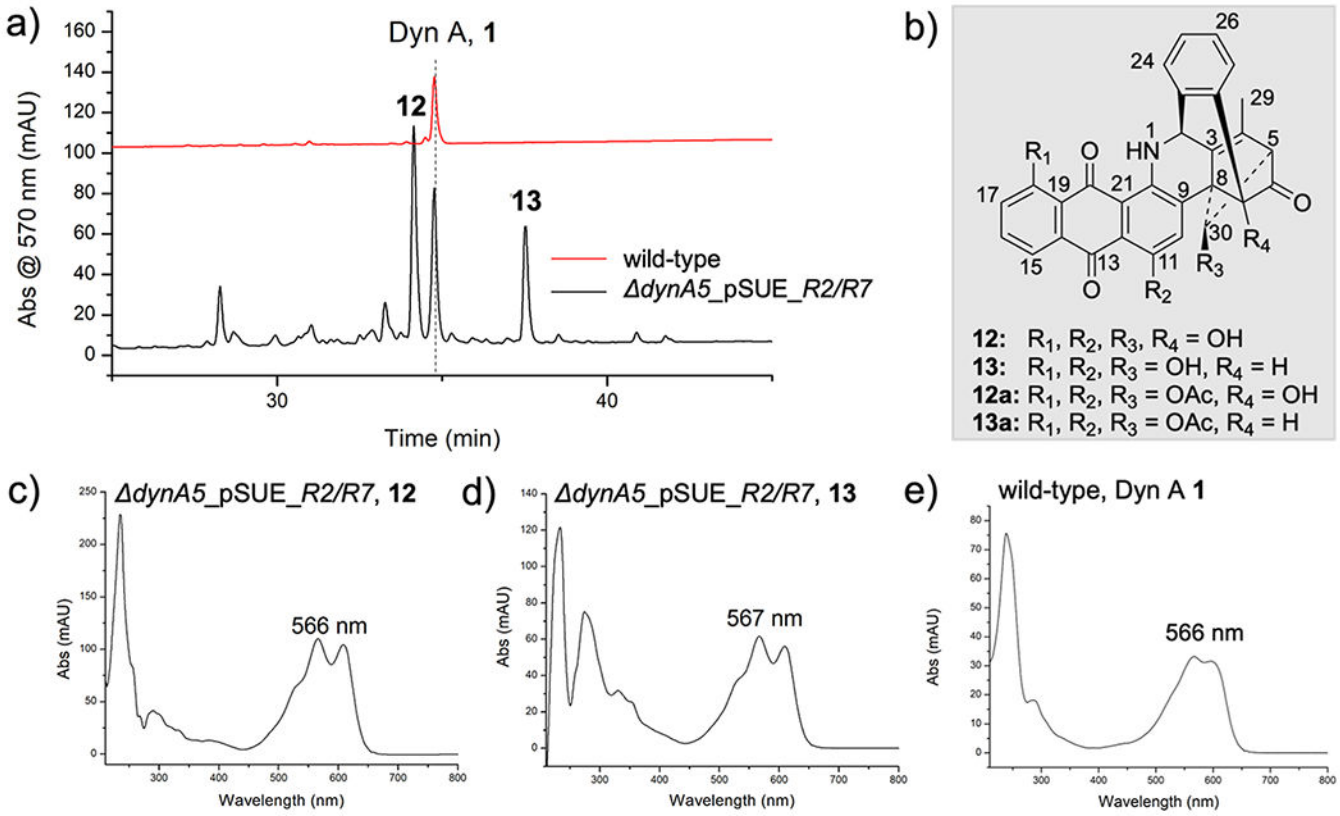

Figure 3.

Comparison of metabolites produced by wild-type *M. chersina* and Δ*dynA5*_pSUE_*R2/R7*. (a) HPLC chromatograms at 570 nm, demonstrating diminished DYN (**1**) production in the Δ*dynA5*_pSUE_*R2/R7* mutant strain and accumulation of **12** and **13** having (b) the indicated structures. (c) UV–visible spectrum of DYN (**1**). (d) UV–visible spectrum of **12**. (d) UV–visible spectrum of **13**.

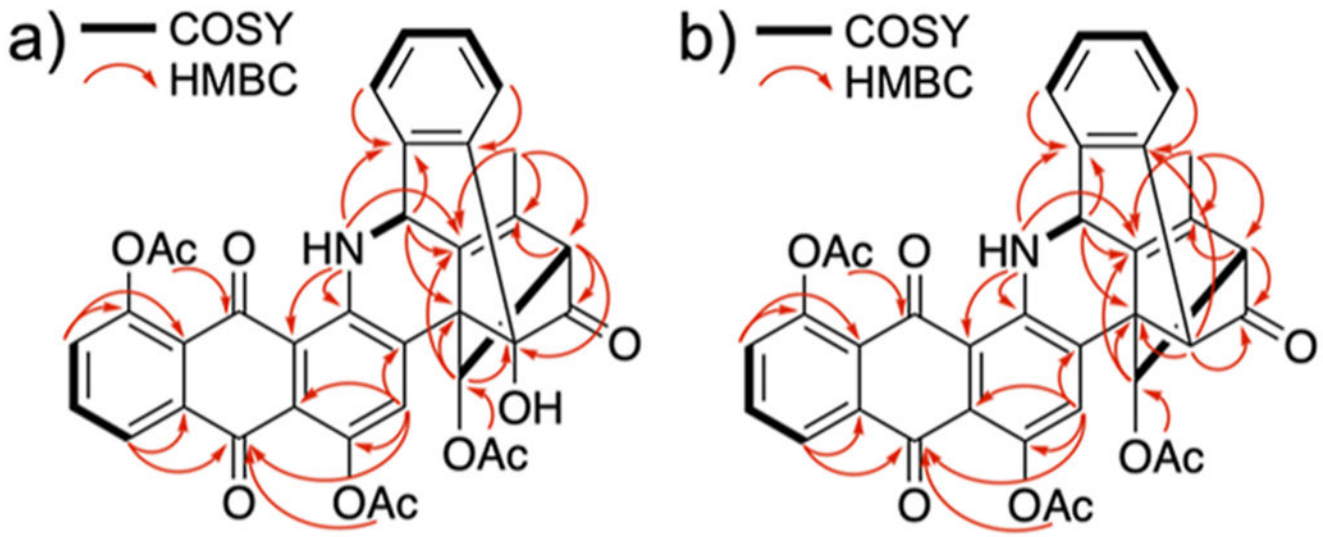

Figure 4.

Structural characterization of **12a** and **13a** by chemical shift correlation, COSY, and HMBC spectroscopy, as indicated.

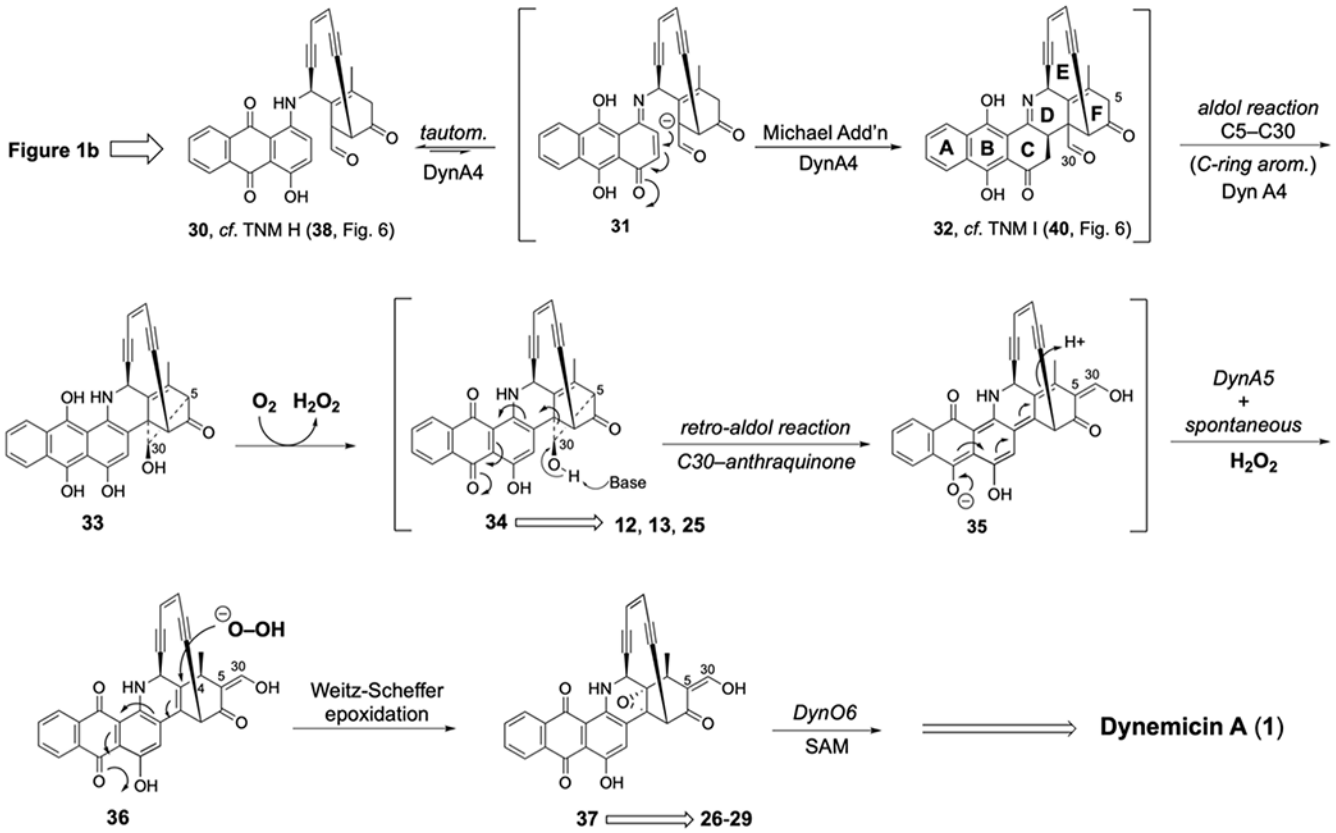

Figure 5.

Biogenetic proposal to dynemicin A (DYN, **1**). Beginning with the DynE8 HR-PKS product **6** and heptaene **7** (Figure 1b), the pathway bifurcates at C_{15} to the heterodimerization of iodoanthracene **8** with an aminoenediyne intermediate **9**, whose structure is not fully known.[9] A mechanism is proposed to complete linking the “upper” and “lower” halves of AFEs from iodoanthracene–γ–thiolactone **8** and a rationale for the last steps of DYN biosynthesis.

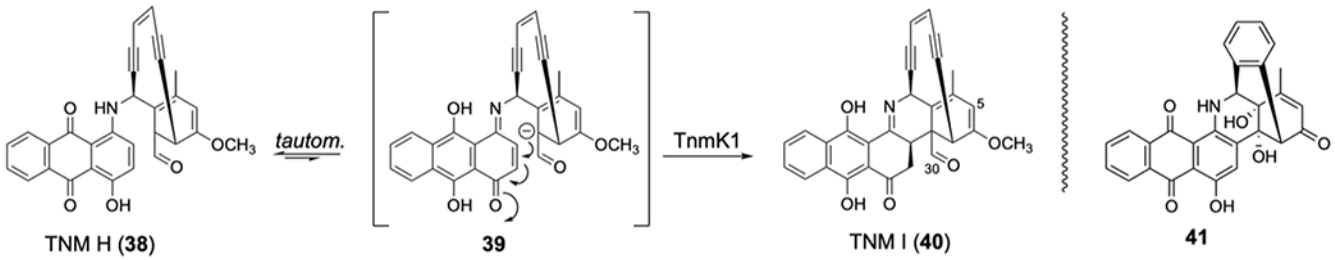

Figure 6.

Proposed mechanism of TnmK1. Heterodimerization to connect the “upper” and “lower” halves of DYN (**1**) is initiated by aryl C–N bond formation to iodoanthracene **8** to give an intermediate resembling the Δ*dynE13* product **19**.[8] Completion of the heterodimerization process by C8–C9 formation is carried out by TnmK1 in the tiancimycin (**3**) biosynthetic pathway and by orthologues in allied AFE pathways. The mechanism illustrated has been proposed to account for the transformation of **38** to **40**.[32]

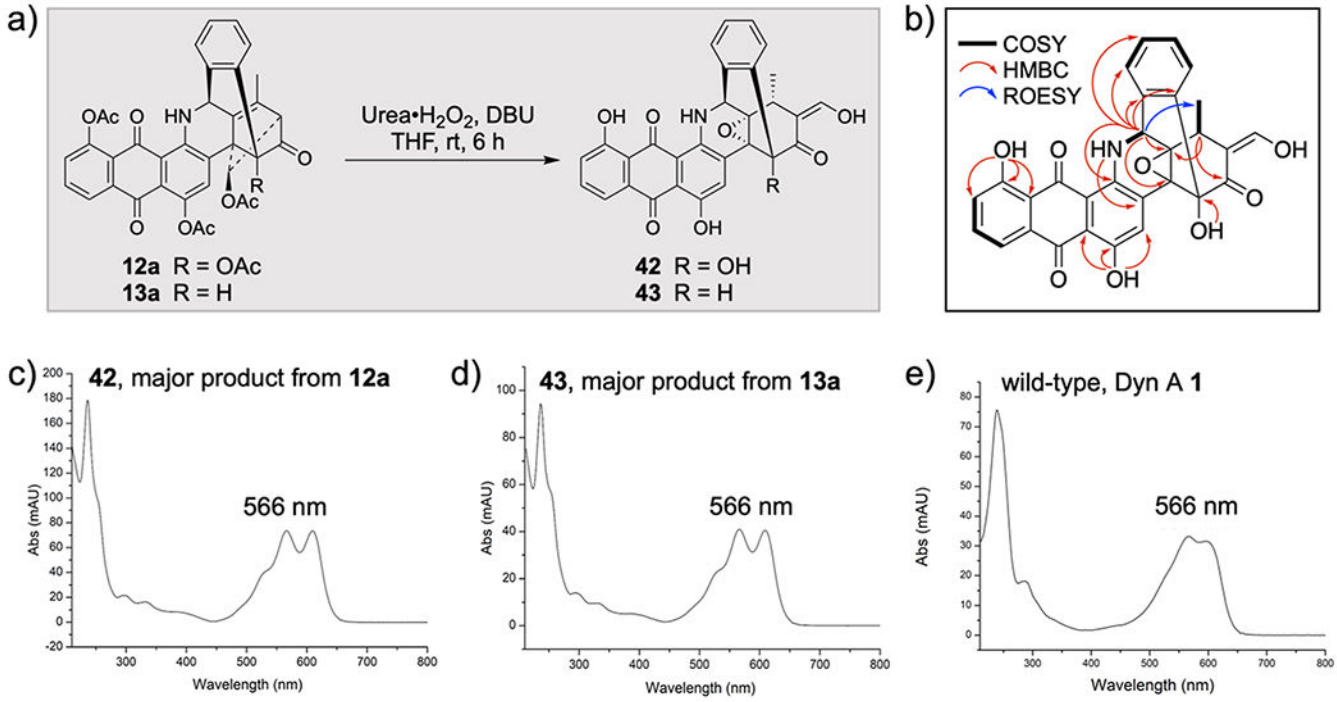

Figure 7.

Biomimetic reaction with compounds **12a** and **13a**. (a) Reaction conditions and indicated structures of the products. (b) Structural characterization of **42** by chemical shift correlation, COSY, HMBC, and ROESY spectroscopy as indicated. (c) UV–visible spectrum of **42**. (d) UV–visible spectrum of **43**. (d) UV–visible spectrum of DYN (**1**).

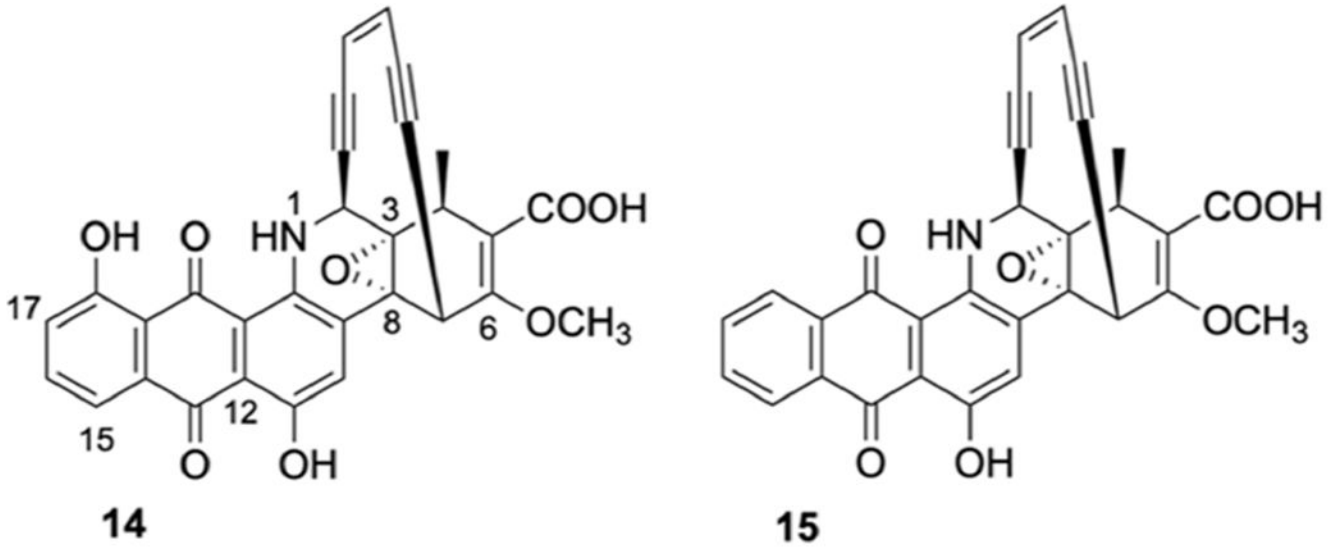

Scheme 1.

A-Ring Deoxygenated Derivatives of DYN from Deletion of *dynE10* Give 14, and Deletion of Both *dynE10* and *dynorf19* Yields 15

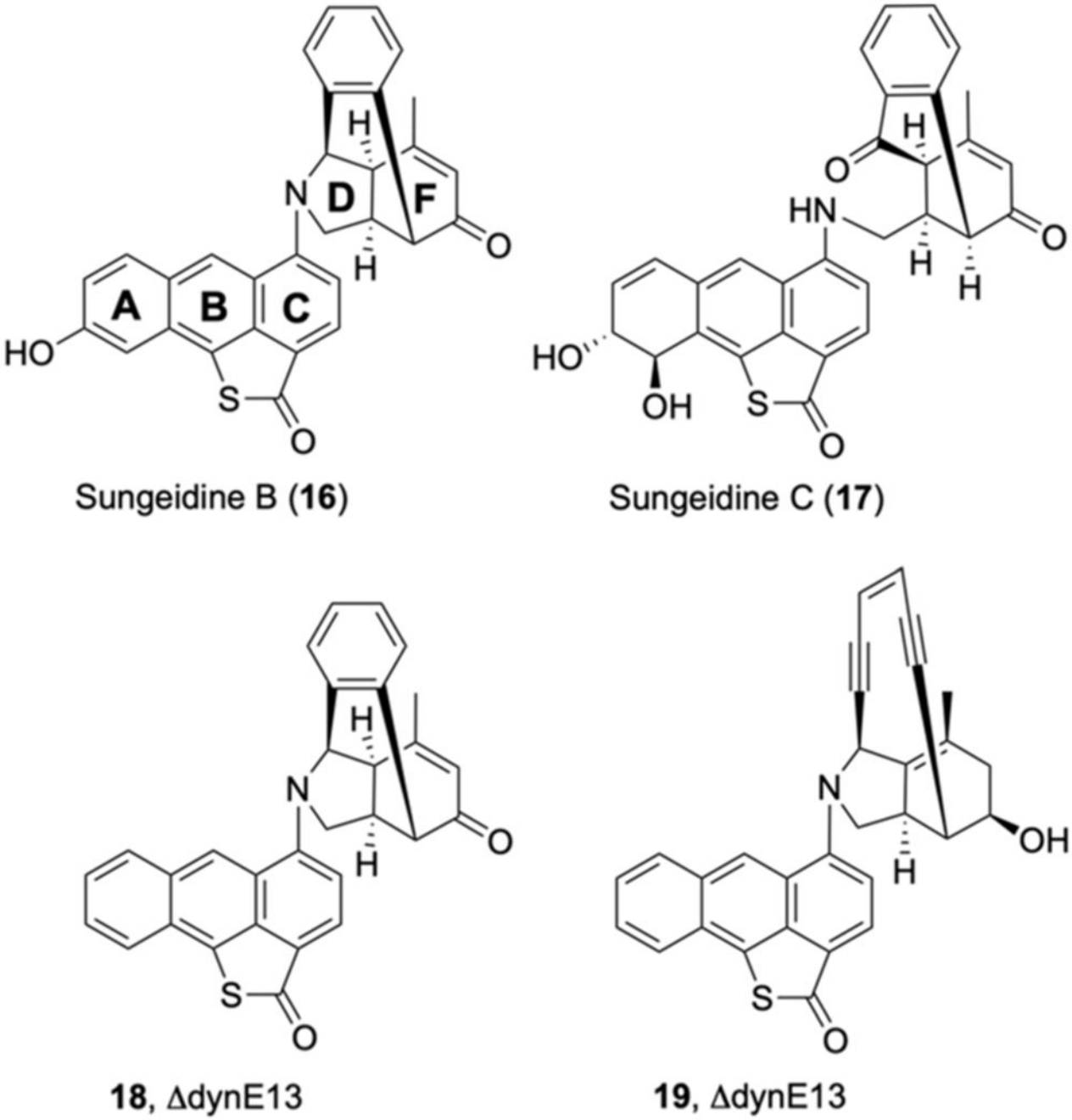

Scheme 2.

Structurally Related Sungeidines B (16), C (17), and Metabolites 18 and 19 that Accumulate in Similar *Micromonospora* Strains Lacking *dynE13* Orthologs

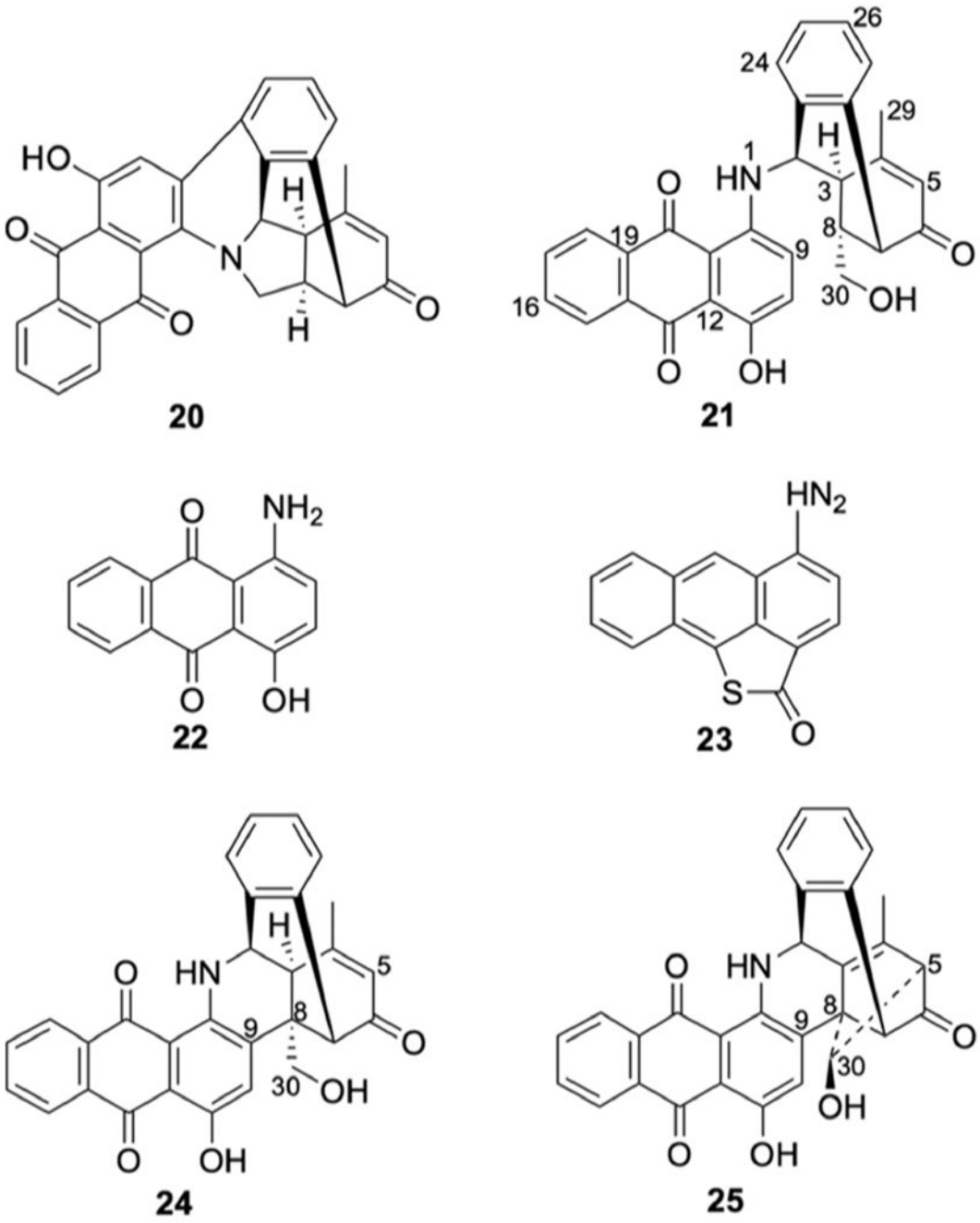

Scheme 3.

Metabolites 20 and 24–25 Accumulated in Gene Reconstitution Experiments Reported in Ma et al.[31] Aminoanthracene 23 is Not an Intermediate in DYN/AFE Biosynthesis[9]

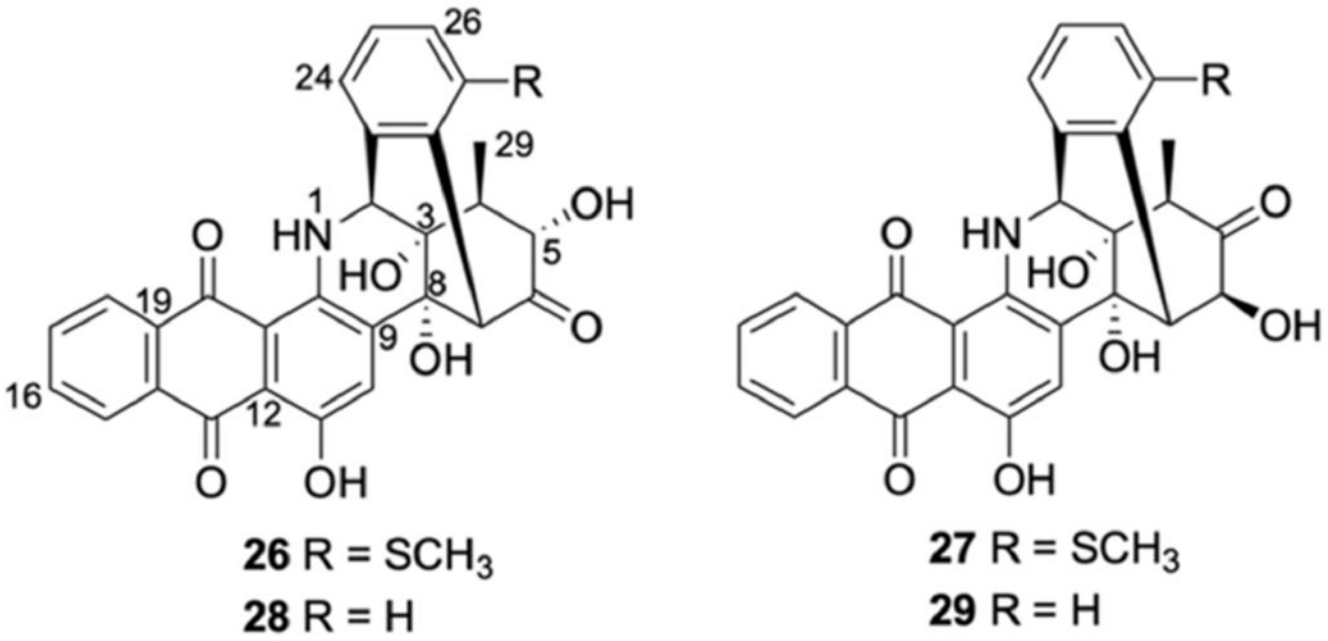

Scheme 4.

Further Metabolites 26–29 Accumulated in Gene Reconstitution Experiments of DYN/AFE Biosynthesis Reported by Ma et al.[31]